



Trans. Nonferrous Met. Soc. China 24(2014) 1058-1064

Transactions of **Nonferrous Metals** Society of China

www.tnmsc.cn

Surface modification of biomedical magnesium alloy wires by micro-arc oxidation

Cheng-lin CHU¹, Xiao HAN¹, Jing BAI¹, Feng XUE¹, Paul-kao CHU²

- 1. Jiangsu Key Laboratory for Advanced Metallic Materials, School of Materials Science and Engineering, Southeast University, Nanjing 211189, China;
 - 2. Department of Physics and Materials Science, City University of Hong Kong, Tat Chee, Avenue, Kowloon, Hong Kong, China

Received 27 April 2013; accepted 3 September 2013

Abstract: Magnesium alloy wires were processed by micro-arc oxidation (MAO) in a modified silicate-phosphate composite electrolyte containing hydroxyapatite (HA) nanopowders and NaOH. Effects of NaOH content in the composite electrolyte on the microstructure and properties of the MAO ceramic coatings on magnesium alloy wires were studied. It is found that the arc voltage of magnesium alloy wires in the micro-arc oxidation process is significantly reduced while the oxidation rate is accelerated. Addition of 2 g/L NaOH in the composite electrolyte is a better choice for improving corrosion resistance of magnesium alloy wires. During early simulated body fluids (SBF) immersion, the micro-arc oxidized magnesium alloy wires undergo a slow and stable degradation. After soaking for 28 d, the protective ceramic coating still shows no damage but significant degradation is observed for magnesium alloy wires after immersion for more than 60 d.

Key words: magnesium alloy wire; hydroxyapatite; micro-arc oxidation; corrosion resistance

1 Introduction

Magnesium alloys with a low density, high specific strength, good biocompatibility, and in vivo degradation characteristic are ideal degradable biomaterials [1-4]. However, their poor corrosion resistance can lead to a fast degradation accompanied by rapid release of hydrogen gas thereby hampering medical applications [5,6]. Surface modification can improve the corrosion resistance and control the degradation rate of magnesium alloys [7–12]. Micro-arc oxidation (MAO) which is suitable for magnesium alloys [13-16] can produce thick ceramic coatings with high interfacial bond strength and efficiency. In MAO, the composition of the electrolyte is very important. The silicate, phosphate, aluminate, or combination electrolytes have been mainly used for magnesium alloys, and addition of other chemicals into the electrolytes can improve the microstructure and properties of the MAO coatings. For example, ceramic coatings containing Ca and P can be synthesized on

magnesium alloys in an electrolyte with calcium and phosphate salts [17], and adding glycerol and Na₂EDTA into the electrolyte can significantly reduce the point discharge phenomenon and lead to steady formation of the ceramic coating [18]. In addition, addition of some peroxides such as H₂O₂ to the electrolyte increases the supply of oxygen and expedites the MAO process [19].

Wires made of biodegradable magnesium alloys can replace some traditional metallic wires made of titanium alloys and stainless steels in next-generation absorbable gastrointestinal brackets, cardiovascular stents, and orthopedic devices. The biodegradable property of magnesium wires eliminates risks arising from the long-term presence of the implants in vivo and subsequent surgeries for removal. There is both scientific and technical interest in investigating the effects of MAO on the microstructure of the ceramic coating as well as corrosion resistance and biological performance of medical magnesium alloy wires, although a systematic study has not been conducted. In this work, a silicate-phosphate composite electrolyte containing hydroxyapatite (HA) nanopowders and sodium hydroxide is employed to reduce the arcing voltage in MAO and improve the microstructure and properties of the protective ceramic coatings. The effects of the NaOH content on the microstructure of the ceramic coatings and the corrosion resistance and degradation behavior of the materials are investigated systematically in simulated body fluids (SBF).

2 Experimental

2.1 Micro-arc oxidation

The AZ31B magnesium alloy wires with a diameter of 0.30 mm were drawn, annealed, gently ground with 2000# SiC sandpaper, washed with acetone, distilled water, and ethanol sequentially, and cleaned ultrasonically three times. The WHD-30 type micro-arc oxidation powder was used in MAO with the magnesium alloy wires acting as the anode and stainless steel sink as the cathode. The samples were held and suspended in the electrolyte during MAO at temperature of 20-40 °C. After MAO for a predetermined duration, the specimen was removed and washed with deionized water.

Based on our preliminary studies, the electrolyte composed of sodium silicate (10 g/L), sodium phosphate (5 g/L), and uniformly-dispersed HA nanoparticles (3 g/L) with a diameter of about 100 nm by ultrasonic vibration was used. Different concentrations of sodium hydroxide (1 g/L to 4 g/L) were added to the electrolyte. The constant voltage mode with a forward voltage of 400 V and negative voltage of 40 V was adopted and the oxidation time was 15 min.

2.2 Microstructural characterization

The Philips XL30 FEG scanning electron microscope (SEM) and FEI SIRION field-emission SEM were used to characterize the surface morphology and thickness of the coating. The elemental composition of the coatings was determined by energy-dispersive X-ray spectroscopy. The Bruker D8-Discover X-ray diffractometer (XRD) was used to determine the phases in the coatings using the following conditions: Cu K_{α} radiation, wavelength of 0.15418 nm, acceleration voltage of 40 kV, current of 30 mA, scanning step of 0.02 (°)/step, and scanning speed of 2 s/step. The measured angle error was less than $\pm 0.01^{\circ}$.

The Philips XL30 FEG SEM was used to obtain five random photographs of the surface morphology from each sample and the Image-Pro software was used to measure the pore diameters. In a typical process, the diameters of 20–30 pores were randomly measured from each photograph and the average pore diameter based on all five photographs was calculated to represent the pore size of each sample surface. The region with a

black-and-white contrast between 50 to 199 was selected as the flat area and the ratio of the flat area to the total area was calculated.

2.3 Electrochemical measurements

The potentiodynamic polarization tests were performed on the Princeton Applied Search (PAR) PARSTAT2273 electrochemical workstation consisting of a three-electrode system with the saturated calomel electrode as the reference electrode, platinum foil as the auxiliary electrode, sample as the working electrode, and simulated body fluid (SBF) as the corrosion medium. The SBF solution was buffered at pH 7.4 with trimethanol aminomethane-HCl. The ionic concentrations in the SBF solution were nearly equal to those in human body blood plasma as follows: 142.0 mmol/L Na⁺, 5.0 mmol/L K⁺, 2.5 mmol/L Ca²⁺, 1.5 mmol/L Mg²⁺, 4.2 mmol/L HCO₃ , 148.5 mmol/L Cl⁻, 1.0 mmol/L HPO_4^{2-} and 0.5 mmol/L SO_4^{2-} . The electrochemical parameters were as follows: scanning interval starting at the corrosion potential below 250 mV and terminating at higher than 800 mV and scanning speed of 1 mV/s. In general, the smaller the corrosion current density is, the more positive the corrosion potential is, and the better the resistance to the uniform corrosion is.

2.4 Immersion tests

Three 3 cm-long magnesium alloy wires were used in the SBF immersion test. Each wire was placed in a polyethylene bottle with 15 mL of SBF and put in a thermostat oscillation slot at a temperature of (37.5±0.5) °C. Immersion was carried out for 1–90 d. The SBF was replenished once a day. After soaking for the predetermined time, the magnesium alloy wires were taken out from the bottle and the pH value of SBF was determined. The surface morphology and phase composition of the magnesium alloy wires were also determined.

3 Results and discussion

3.1 Microstructure of MAO ceramic coatings

Figure 1 depicts the representative photo of the magnesium alloy wire and sheet after MAO, confirming that they are covered by a white and uniform protective ceramic coating. The arcing voltage in MAO after addition of sodium hydroxide into the electrolyte is reduced significantly to below 200 V thus accelerating coating formation. Using the same electrical parameters but without NaOH, the arcing voltage exceeds 350 V and the total coating thickness is only 7.1 µm. In comparison, after addition of sodium hydroxide, the thickness of the MAO ceramic coating increases with NaOH contents reaching 25.3 µm when the NaOH concentration is 4 g/L,

as shown in Fig. 2. The MAO coating on magnesium normally comprises a porous surface layer and dense inner layer. Our results show that the growth trend is different for these two layers as the NaOH concentration goes up. For instance, for 1 g/L NaOH, the dense layer has a thickness of 10.6 µm whereas the porous layer is 6.7 µm thick. When the NaOH concentration is increased to 2 g/L, the thickness of the dense layer does not change but that of the porous layer increases to 8.3 µm. As the NaOH concentration is increased to 3 g/L and 4 g/L, the porous layer thickness increases rapidly to 15.9 and 18.4 μm, respectively, but that of the dense layer decreases to 6.5 to 6.9 µm. With increasing NaOH concentration, the starting arc voltage is reduced. Hence, for the same applied voltage, the breakdown energy for the coating increases while the oxides participating in the melting and sintering process are gradually increased. The overall MAO coating thickness increases. Our data reveal that the deposition rate is increased by adding more NaOH to the electrolyte. However, when the NaOH concentration is increased to 3 or 4 g/L, the thickness of the dense layer



Fig. 1 Optical picture of magnesium alloy wire (left) and sheet (right) after MAO

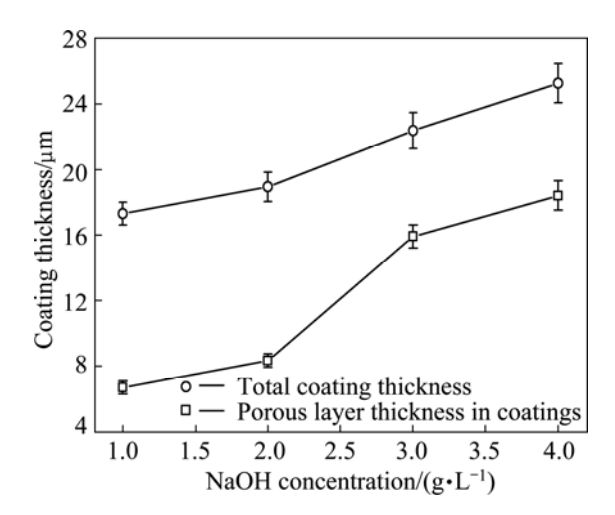


Fig. 2 Coating thicknesses on magnesium alloy wires after MAO in electrolyte containing different concentrations of NaOH

does not increase and even decreases. During MAO, energy accumulation and repeated breakdown with increasing NaOH content in the electrolyte can lead to remelting of the dense film and generation of the pores with some discharge channels.

Figure 3 shows the surface morphology of the MAO coatings produced with different concentrations of NaOH. The average pore size and surface flatness of the coatings are listed in Table 1. With increasing NaOH concentration, the amount and diameter of the pores increase and parts of the circular pores morph into interconnected ones. With increasing NaOH concentration, the conductivity of the electrolyte is improved and the sparks generated in the reaction become more intense. Thus the number of micro-arcs in a unit time increases significantly, thus leading to an increase in the micro-arc pores on the sample surface. However, when the NaOH concentration is increased further, although the electrical conductivity of the electrolyte continues to improve, the electrolyte temperature increases rapidly due to the heat generated in the vicinity of the electrode. This is not conducive to the timely condensation of the micro-arc discharge holes. With continuous breakdown of the formed film, the micro-arc pores continue to expand and increase, as shown in Fig. 3(d). The micro-arc discharge holes change from a round structure to an elongated ellipse or stripe. As the NaOH concentration is increased, the surface flatness of the coatings also changes. For 1 g/L NaOH, the surface flatness is 20.32%. As shown in Fig. 3 and Table 1, although the surface pores are relatively small, there are some discharge zones and grooves on the surface giving rise to the contrast in the SEM images. When the NaOH concentration is increased to 2 g/L or more, although the pore size of the surface increases, the surface flatness is improved.

Figure 4(a) shows the XRD patterns of the magnesium alloy after MAO. The coating is composed of mainly periclase-type MgO, but small amounts of MgSiO₃ and hydroxyapatite phases can also be observed. Since the coating is thin, XRD also detects the magnesium alloy substrate. As the oxidation process progresses, rapid release of large energy leads to micromelting on the surface. The MgO phase is thus quickly generated as oxygen is attracted to the anode under the cooling effect of the electrolyte. The presence of MgO phase with a high melting point of 2800 °C indicates that the micro-arc area must have a very high temperature. The small amount of hydroxyapatite phase in the MAO ceramic coating may be attributed to the addition of hydroxyapatite nanoparticles to the electrolyte.

3.2 Corrosion and degradation behavior

Figure 5 shows the potentiodynamic polarization

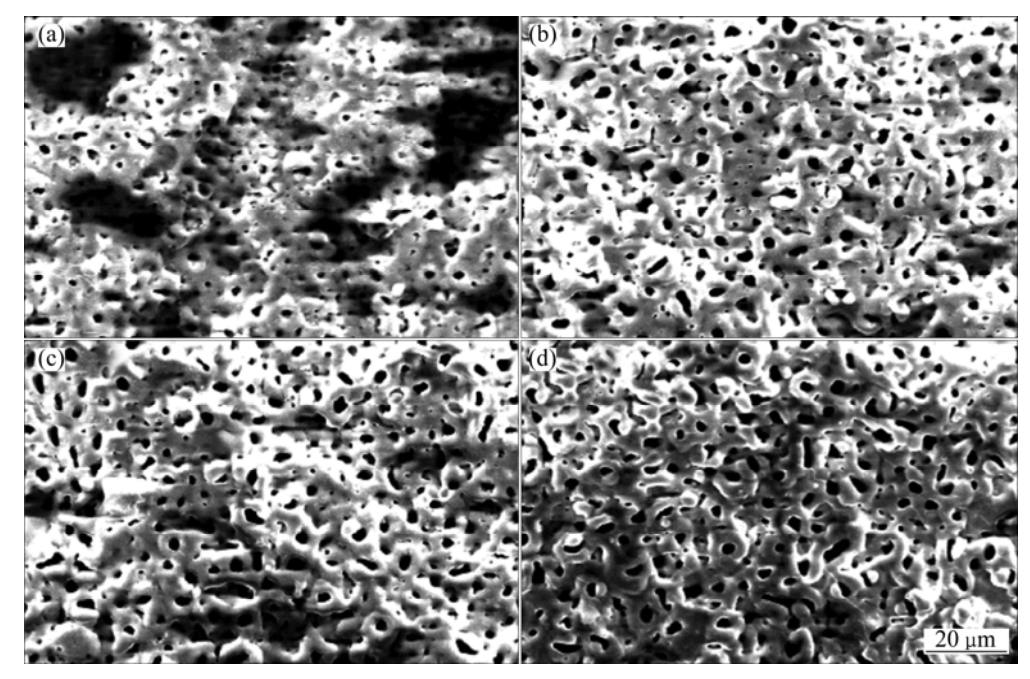


Fig. 3 SEM images of magnesium alloys treated with different concentrations of NaOH: (a) 1 g/L; (b) 2 g/L; (c) 3 g/L; (d) 4 g/L

Table 1 Surface pore size and flatness of magnesium alloys treated in electrolytes with different concentrations of NaOH

NaOH concentration/	Average	Surface
$(g \cdot L^{-1})$	pore size/μm	flatness/%
1	2.5±0.1	20.3±1.1
2	3.8±0.2	41.4±2.0
3	3.9±0.2	37.3±1.8
4	4.7±0.2	56.3±2.4

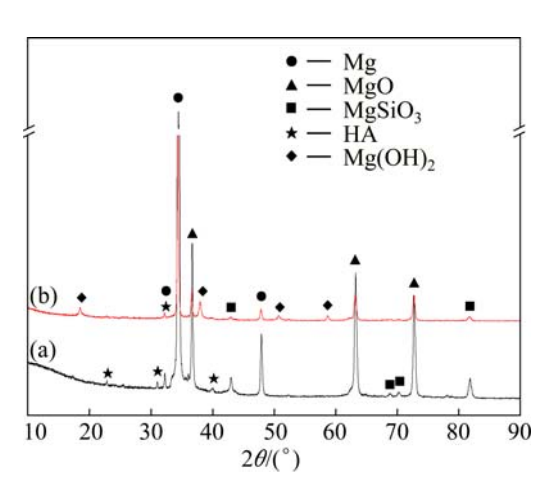


Fig. 4 XRD patterns of micro-arc oxidized magnesium alloys before (a) and after (b) immersion test in SBF for 28 d

curves of the magnesium alloy wires treated with different concentrations of NaOH. The corresponding corrosion potential and corrosion current density are listed in Table 2. The sample treated with 2 g/L NaOH has a higher corrosion potential, indicating that it is less susceptible to electrochemical corrosion.

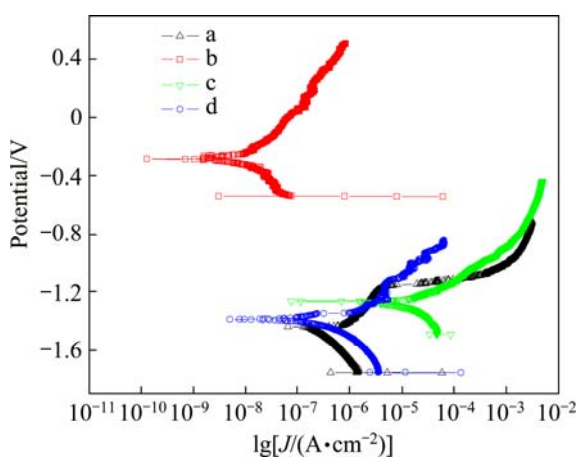


Fig. 5 Potentiodynamic polarization curves of magnesium alloy wires treated with different concentrations of NaOH: (a) 1 g/L; (b) 2 g/L; (c) 3 g/L; (d) 4 g/L

Table 2 Potentiodynamic polarization analysis of magnesium alloy wires treated with different concentrations of NaOH

NaOH concentration/ (g·L ⁻¹)	$\varphi_{ m corr}$ /V	$J_{\rm corr}/(\mu {\rm A\cdot cm}^{-2})$
1	-1.44	0.21
2	-0.29	0.0104
3	-1.26	10.5
4	-1.39	1.00

This sample also has a smaller corrosion current density (J_{corr}) , which indicates that during the corrosion process, the electrochemical reaction is relatively slow and so it has the best corrosion resistance. By taking into account the surface flatness, pore size, film thickness, and corrosion resistance, addition of 2 g/L NaOH is optimal.

After the samples are immersed in SBF for different periods, the degradation behavior is evaluated by visual observation and SEM. Within the first 4 d, the untreated AZ31B magnesium alloy wires are broken and some white substances appear on each residual short wire. As the immersion time is prolonged, the residual magnesium alloy wires continue to corrode and break into smaller pieces. Our data show that the untreated Mg alloy wires degrade very fast and cannot meet clinical requirements. In comparison, Fig. 6 shows the low-magnification surface morphology of MAO magnesium alloy wires after immersion in SBF for different periods. After immersion for 14 d, the macroscopic morphology of the wires does not change significantly, as shown in Figs. 6(a) and (b). Even after 28 d, the ceramic coatings on the MAO magnesium alloy wires remain intact, although some micro-cracks and a small amount of deposition products can be observed from Fig. 6(c). However, after Fig. 6(d), although no fractures 60 d, as shown in can be observed, the surface shows damage and some corrosion pits appear. Immersion for a longer period reveals severe degradation after 60 to 75 d.

Figure 7 shows the high-magnification surface morphology of the MAO magnesium alloy wires after immersion in SBF for different periods. After 4 d, some flocculent corrosion products are attached to the broken wire surfaces without MAO treatment. After 7 d, the surface roughness on the untreated wires increases and some micro-cracks extend and cross-link into a ditch throughout the sample surface. On the other hand, only small cracks appear from the surface of the MAO sample. After 14 d, its surface flatness degrades seriously and corrosion products including spherical ones are found on the surface, indicating that the corrosion cracks have

extended into the samples. In contrast, at this juncture, the surface micro-cracks on the treated sample do not deteriorate and the surface remains smooth without damage. After 28 d, some larger and deeper micro-cracks appear on the MAO sample. After 60 d, serious damage is observed from the MAO wires. The wall of the corrosion pits is porous and there is corrosion cracking which indicates severe corrosion.

Figure 4(b) shows the XRD pattern of the MAO sample after immersion in SBF for 28 d. Clearly, Mg, MgO and Mg(OH)₂ are the main phases and a small amounts of MgSiO₃ and HA can also be observed. Compared with Fig. 4(a), the new phase Mg(OH)₂ is the degradation product, whereas the original MgO, HA and MgSiO₃ phases in the ceramic coating are reduced after immersion due to degradation. All in all, the corrosion resistance of the MAO samples is better and the degradation behavior is attributed to the protective effects rendered by MgO, HA, and MgSiO₃ in the MAO coating.

The pH values of the SBF change with immersion time as shown in Fig. 8. Since the SBF is changed every day, the results in Fig. 8 show the daily interaction between the SBF and samples at different immersion stages. During immersion, the degradation products are released slowly from the sample surface to the SBF. Meanwhile, some substances are deposited on the sample surface from the SBF. Both processes alter the ion concentrations and pH of the SBF. Hence, Fig. 8 indirectly reflects the degradation rates of the magnesium alloy wires. During the initial immersion, the pH values of the SBF for both samples are higher than the initial values. At the same immersion time, the pH change observed from the untreated sample is larger, indicating

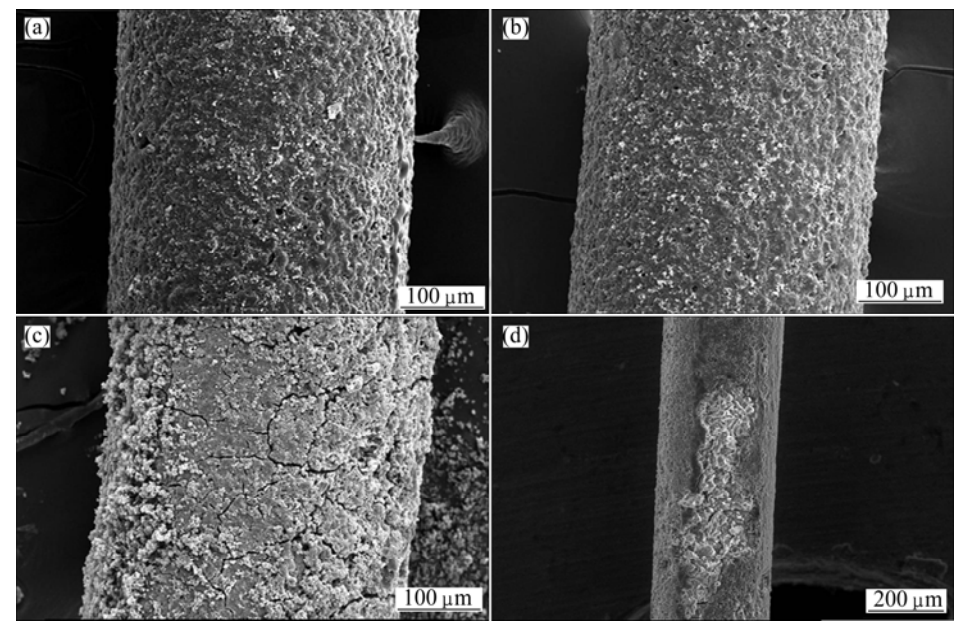


Fig. 6 Low-magnification SEM images of MAO magnesium alloy wires immersed in SBF for different periods: (a) 7 d; (b) 14 d; (c) 28 d; (d) 60 d

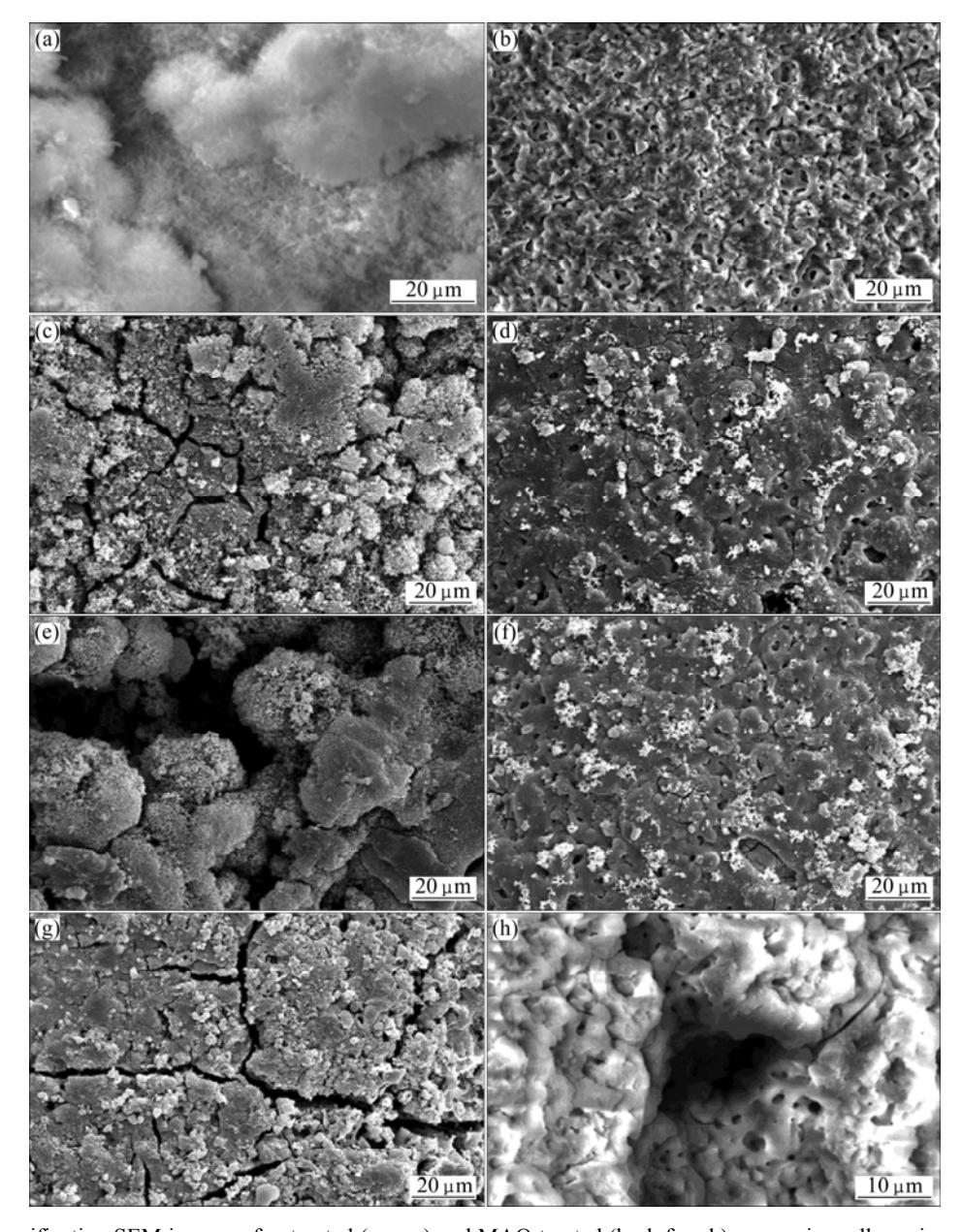


Fig. 7 High-magnification SEM images of untreated (a, c, e) and MAO treated (b, d, f, g, h) magnesium alloy wires after immersion for different periods: (a, b) 4 d; (c, d) 7 d; (e, f) 14 d; (g) 28 d; (h) 60 d

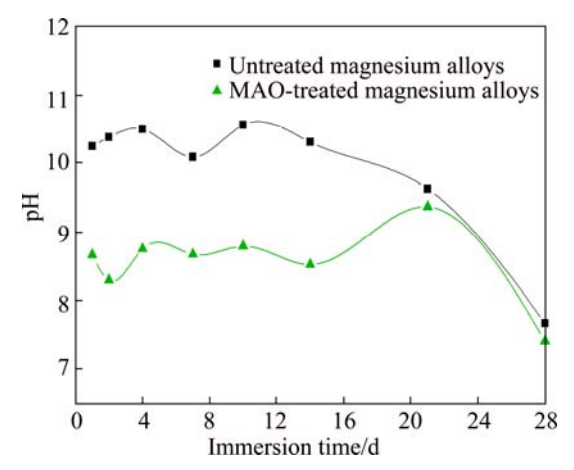


Fig. 8 Changes in pH values of SBF with immersion time for different samples

larger corrosion rate and higher susceptibility to corrosion. After MAO, the magnesium alloy wire is covered and protected by the ceramic coating. Thus, the corrosion behavior of the wire is altered but it is associated with a relatively small change in the SBF pH. That is, in the early immersion stage, the MAO wire undergoes slow and stable degradation, resulting in a very small pH change in the surrounding physiological environment, thus boding well for applications in vivo.

4 Conclusions

By using a silicate-phosphate electrolyte containing hydroxyapatite nanopowders and sodium hydroxide, the arcing voltage during MAO is reduced significantly while the oxidation rate is increased. As the sodium hydroxide content increases, the porous oxide layer is thicker but the thickness of the inner dense layer in the ceramic coating is unchanged or even decreases. The magnesium alloy wire treated with 2 g/L NaOH has the highest corrosion potential and smallest corrosion current density, thereby reflecting better corrosion resistance. The MAO coating is composed of mainly the periclasetype MgO phase in addition to small amounts of MgSiO₃ and HA phases. After immersion in SBF, the Mg(OH)₂ phase emerges as the degradation product. In SBF, the untreated AZ31B magnesium alloy wires exhibit a fast degradation rate but MAO can effectively improve the corrosion resistance and control its degradation behavior. During early immersion, the MAO wires show slow and stable degradation and even after immersion for 28 d, the ceramic coating shows no damage. However, significant degradation is observed from the MAO magnesium alloy wires after immersion for more than 60 d.

References

- STAIGER M P, PIETAK A M, HUADMAI J, DIAS G. Magnesium and its alloys as orthopedic biomaterials: A review [J]. Biomaterials, 2006. 27: 1728–1734.
- [2] WITTE F. The history of biodegradable magnesium implants: A review [J]. Acta Biomater, 2010, 6: 1680-1692.
- [3] TANJA K, STEFAN F F, ANJA C H, PETER J U, JÖG F L, ANNELIE M W. Magnesium alloys for temporary implants in osteosynthesis: In vivo studies of their degradation and interaction with bone [J]. Acta Biomaterialia, 2012, 8: 1230–1238.
- [4] ZONG Y, YUAN G Y, ZHANG X B, MAO L, NIU J L, DING W J. Comparison of biodegradable behaviors of AZ31 and Mg-Nd-Zn-Zr alloys in Hank's physiological solution [J]. Materials Science and Engineering B, 2012, 177: 395-401.
- [5] GU X N, ZHENG Y F, CHENG Y, ZHONG S P, XI T F. In vitro corrosion and biocompatibility of binary magnesium alloys [J]. Biomaterials, 2009, 30: 484–498.
- [6] XIN Y, HU H, CHU P K. In vitro studies of biomedical magnesium alloys in a simulated physiological environment: A review [J]. Acta Biomaterialia, 2011, 7: 1452–1459.

- [7] HORNBERGER H, VIRTANEN S, BOCCACCINI A R. Biomedical coatings on magnesium alloys: A review [J]. Acta Biomaterialia, 2012, 8: 2442–2455.
- [8] XU L, PAN F, YU G, YANG L, ZHANG E, YANG K. In vitro and in vivo evaluation of the surface bioactivity of a calcium phosphate coated magnesium alloy [J]. Biomaterials, 2009, 30: 1512–1523.
- [9] CHIU K Y, WONG M H, CHENG F T, MAN H C. Characterization and corrosion studies of fluoride conversion coating on degradable Mg implants [J]. Surf Coat Technol, 2007, 202: 590–598.
- [10] WU C, WEN Z, DAI C, LU Y, YANG F. Fabrication of calcium phosphate/chitosan on AZ91D magnesium alloy with a novel method [J]. Surf Coat Technol, 2010, 204: 3336–3347.
- [11] WEN C, GUAN S, PENG L, REN C, WANG X, HU Z. Characterization and degradation behavior of AZ31 alloy surface modified by bone-like hydroxyapatite for implant applications [J]. Appl Surf Sci, 2009, 255: 6433–6438.
- [12] WONG H M, YEUNG K W K, LAM K O, TAM V, CHU P K, LUK K D K. A biodegradable polymer-based coating to control the performance of magnesium alloy orthopaedic implants [J]. Biomaterials, 2010, 31: 2084–96.
- [13] MU W Y, HAN Y. Characterization and properties of the MgF₂/ZrO₂ composite coatings on magnesium prepared by micro-arc oxidation [J]. Surface & Coatings Technology, 2008, 202: 4278–4284.
- [14] GU X N, LI N, ZHOU W R, ZHENG Y F, ZHAO X, CAI Q Z. Corrosion resistance and surface biocompatibility of a microarc oxidation coating on a Mg-Ca alloy [J]. Acta Biomater, 2011, 7: 1880–1889.
- [15] BARCHICHE C E, ROCCA E, JUERS C, HAZAN J, STEINMETZ J. Corrosion resistance of plasma-anodized AZ91D magnesium alloy by electrochemical methods [J]. Electrochim Acta, 2007, 53: 417–425.
- [16] SRINIVASAN P B, LIANG J, BLAWERT C, STOMER M, DIETZEL W. Characterization of calcium containing plasma electrolytic oxidation coatings on AM50 magnesium alloy [J]. Appl Surf Sci, 2010, 256: 4017–4022.
- [17] YAO Z, LI L, JIANG Z. Adjustment of the ratio of Ca/P in the ceramic coating on Mg alloy by plasma electrolytic oxidation [J]. Appl Surf Sci, 2009, 255: 6724–8.
- [18] GUO H F. Effect of process conditions on micro-arc oxidation of magnesium alloy [J]. Materials Science and Technology, 2006, 14(6): 616–621
- [19] WANG Ping, LI Jian-ping, MA Qun. Optimization of the micro-arc oxidation electrolyte for Mg-9Gd-3Y-0.6Zn-0.5Zr magnesium alloy [J]. Special Casting & Nonferrous Alloys, 2008, 28(7): 502-504. (in Chinese)

医用镁合金丝材的微弧氧化表面改性

储成林1, 韩啸1, 白晶1, 薛烽1, 朱剑豪2

- 1. 东南大学 材料学院, 江苏省先进金属材料重点实验室, 南京 211189; 2. 香港城市大学 物理与材料科学系, 香港
- 摘 要:在硅酸盐-磷酸盐复合电解质中添加羟基磷灰石纳米粉体和氢氧化钠进行改性处理,然后采用该电解质对医用镁合金丝材进行微弧氧化处理。研究电解质中氢氧化钠含量对镁合金丝材表面陶瓷涂层微观组织结构和性能的影响。结果表明:对电解质改性后,镁合金丝材的微弧氧化起弧电压大降低且氧化速度更快。镁合金丝材在添加2g/L氢氧化钠的电解质中进行微弧氧化处理后的耐腐蚀性能改善幅度显著。在模拟体液的早期浸泡过程中,微弧氧化处理过的镁合金丝材表现为缓慢且稳定的腐蚀降解。在浸泡28d后,镁合金丝材表面的保护性陶瓷涂层尚未破坏,但浸泡60d后,镁合金丝材出现了显著的腐蚀降解。

关键词: 镁合金丝材; 羟基磷灰石; 微弧氧化; 耐腐蚀性能